



Contents lists available at ScienceDirect

Combustion and Flame

journal homepage: www.elsevier.com/locate/combustflame

Experimental study of temperature influence on carbon particle formation in shock wave pyrolysis of benzene and benzene–ethanol mixtures

Alexander Eremin^a, Evgeny Gurentsov^a, Ekaterina Mikheyeva^{a,b,*}^a Joint Institute for High Temperatures, Russian Academy of Sciences, Moscow, Russia^b Bauman Moscow State Technical University, Moscow, Russia

ARTICLE INFO

Article history:

Received 28 June 2014

Received in revised form 17 September 2014

Accepted 22 September 2014

Available online xxxx

Keywords:

Soot formation

Benzene–ethanol pyrolysis

Shock wave hydrocarbon pyrolysis

Soot diagnostics

ABSTRACT

The carbon particle formation process in a pyrolysis of benzene and benzene–ethanol mixtures diluted by argon at initial temperatures 1650–2600 K and pressures 1.4–5.5 bar behind reflected shock waves was studied. The manifold optical diagnostics: emission–absorption spectroscopy for gas–particle temperature, time-resolved laser-induced incandescence (Ti-Re LII) for particle size evaluation and laser light extinction for the volume fraction of condensed phase measurements were applied simultaneously. The temperature in pyrolysis process was found to differ significantly from the initial temperature behind the reflected shock wave in all studied mixtures. The real temperature dependences of volume fraction of condensed phase at the wavelength of 633 nm and particle size based on the performed measurements were specified and analyzed. The effect of ethanol addition on carbon particle formation and reaction temperature in benzene pyrolysis is discussed.

© 2014 The Combustion Institute. Published by Elsevier Inc. All rights reserved.

1. Introduction

One of the major problems in combustion is the reduction of particulate carbon emission. The key point to study this problem is the investigation of the processes of condensed carbon particle formation. It is generally known that carbon particles, usually attributed to soot, have a core consisting of polyaromatic hydrocarbons (PAH). Benzene molecule represents a first aromatic ring and it is considered as one of the initial steps towards PAH growth [1].

The reactive temperature is crucial parameter for soot formation process. The well-known bell-shaped temperature dependences of soot yield and the particle size were observed in shock wave pyrolysis and flames [2,3]. In benzene the shift of about 200 K of the top of bell-shaped temperature dependence of soot yield towards higher temperatures was found with increasing of benzene concentration from 0.5% to 2% [2], the shift to the lower temperature was observed in pyrolysis of 0.5–1.5% toluene in argon [4]. However there is no kinetic reason for the change in temperature dependence of the soot yield with varying initial hydrocarbon concentration. Note that the reaction temperature

in majority of shock tube studies was assumed equal to the initial temperature behind the front of the reflected shock wave (so-called frozen temperature) due to high dilution in bath gas. In [3] it was supposed that the reason of the apparent change of bell-shaped curve position is the difference of the reaction temperature from the frozen temperature due to heat consumption or release at the initial steps of pyrolysis. The difference of the reaction temperature at shock wave pyrolysis of ethylene from its initial value behind the front of shock wave was predicted in [5]; besides that similar effect was experimentally observed in pyrolysis of carbon suboxide [6], acetylene, n-hexane, and benzene [7]. Therefore the correct determination of the real temperature during soot formation process could impact not only on the rates of chemical reactions, but also on the interpretation of the measurements of carbon particle yield under various conditions.

The oxygenated additions are expected to decrease a condensed carbon formation. Ethanol is widely produced from biomass and it is a promising substance as an additive to the fuels. The suppression effect of 0.31% of ethanol addition on PAH and soot formation was found in a shock wave pyrolysis of 0.31% benzene in argon [8] and in premixed fuel-rich ethylene–air flames by addition ethanol of 5% and 10% in oxygen by weight in the fuel [9]. In these studies the essential inhibition effect was explained by the increase of oxidation rate of carbon particles and their precursors. Another route of suppression effect of ethanol additives is the formation

* Corresponding author at: Joint Institute for High Temperatures, Russian Academy of Sciences, Izhorshkaya 13, Moscow 125412, Russia. Fax: +7 (495) 495 79 90.

E-mail address: mikheyeva@ihed.ras.ru (E. Mikheyeva).

of H₂O after decomposition of ethanol and consequent consumption of hydrogen atoms, that promote HACA mechanism of surface growth of carbon particles, with production of OH and H₂ [8]. On the other hand, a small amount – 10% replacement of benzene by oxygenated additives (MTBE, methanol, ethanol, isobutene) can promote the carbon particle formation due to peculiarity of the kinetics of blend pyrolysis [10]. The experimental study [4] showed an increase of soot amount in shock tube pyrolysis of 1% toluene + (1–3)% ethanol mixtures. The increase of carbon particle yield with 2–9% replacement of ethylene by ethanol in non-premixed ethylene flame was observed in [11]. These results are in conflict with suppression effect of ethanol admixture in shock tubes [8] where the decomposition of initial hydrocarbon occurs due to pyrolysis process that is similar to non-premixed flame conditions. Besides the uncertainty in the mechanism of ethanol suppression effect on carbon particle yield, no attention was paid to the reaction temperature influence on the pyrolysis of hydrocarbon–ethanol mixtures.

The present study was focused on the actual temperature behavior and the resulting temperature influence on the carbon particle formation process during pyrolysis of (1–2)% benzene and 1% benzene + (1–3)% ethanol diluted in argon. The main merit of this study is the simultaneous measurements of carbon particle size, volume fraction and current reaction temperature.

2. Experimental methods

2.1. Shock tube

The experiments were performed behind reflected shock waves in a conventional diaphragm type shock tube with an inner diameter of 50 mm (Fig. 1). After the each experiment the shock tube has been cleaned by alcohol to remove the water from the shock tube walls. The shock tube was evacuated down to the pressure of 10^{−2} Torr by a fore-vacuum pump before every run. The test gas mixtures were prepared manometrically in a mixing vessel. The gases with the purity of 99.9% for benzene, 99.999% for argon and 95% water solution of ethanol were used. In case of benzene and ethanol the saturated vapors for mixture compounding at room temperature without extra heating were used. The blends were kept in mixing vessel for at least an hour before the experiment. The investigated mixtures and ranges of experimental conditions are listed in Table 1. The data of each shock tube experiment are listed in supplement material #1. The initial temperature T_5 and the pressure P_5 behind the front of the reflected shock wave were determined based on measured incident shock wave velocity by applying one-dimensional gas-dynamic theory with the assumption of “frozen” reaction conditions. An inaccuracy of the temperature T_5 calculation was about 1–1.5% for all range of experiments and was caused by an uncertainty of incident shock wave velocity measured by three pressure transducers. The optical access to the measurement section was given by four calcium fluoride windows of 6 mm in a diameter, mounted perpendicular to each other at the distance of 45 mm from end flange of the shock tube.

2.2. Gas-particle temperature measurements

The emission–absorption spectroscopy was applied for the time-resolved temperature measurements during the pyrolysis of hydrocarbons. This method is based on simultaneous detection of emission and absorption of reactive mixture at the same wavelength [12]. The measurements were carried out by two identical optical channels that focus the light from the probe region via the pair of the calcium fluoride windows installed in a horizontal plane of the shock tube and further via lenses onto two photomul-

tipliers (Fig. 1b). The first channel registered an emission only. The second channel was exposed to radiation from reference source with known brightness temperature. Thus the second channel detected the combination of absorption and emission of reaction mixture. The optical arrangement allowed changing the channels to check their volume identity. The diaphragm at Fig. 1b had two holes. When both holes are opened and light reference source is turned on, both detectors measure the combination of absorption and emission. When light reference source is turned off, both detectors measure emission only. During the experiment only one hole is opened.

Taking into account Lambert–Beer’s and Kirchhoff’s laws one can get the following expression for the temperature determination:

$$T(t) = \frac{hc}{\lambda k} \left\{ \ln \left[1 + \left(e^{\frac{h}{\lambda k T_0}} - 1 \right) \left(1 - \frac{I_a(t) - I_0}{I_e(t)} \right) \right] \right\}^{-1} \quad (1)$$

here $I_e(t)$ and $I_a(t)$ – are the intensity of time-resolved emission and absorption + emission respectively, h – is the Planck constant, c – is the speed of light, k – is the Boltzmann constant, λ – is a diagnostic wavelength, T_0 – is the brightness temperature of the reference source and I_0 – is the initial intensity of radiation of the reference source.

The main advantage of this temperature measurement technique is that it requires only a calibrated light source, without knowledge of either optical properties of observable reaction mixture or the spectral sensitivity of the detection system. The tungsten ribbon lamp was used as the reference source for absorption channel. The wavelength of 589 nm (centered using a band pass filter with FWHM 20 nm) corresponding to sodium D-line was chosen in order to measure the gas temperature before the condensed phase appearance. The sodium atoms are the inherent natural impurity in argon. Unfortunately, owing to quite low temperatures and insufficient sensitivity of the detection system the emission/absorption signals from sodium atoms were inappropriate for reliable measurements in the most experiments. Thereby the temperature measurements started at the times of appearance of the condensed particles that absorb and emit well in the visible range of spectrum. The carbon particles are assumed to be in the thermal equilibrium with the surrounding gas since the characteristic time needed for the thermal relaxation of nanoparticles with sizes of up to 100 nm with the surrounding gas at atmospheric pressure is less than 1 μ s [13]. The time resolution of the detection system was about 10 μ s, the space resolution was 3 mm. In Fig. 2 the example of measured emission/absorption signals (a) and corresponding calculated temperature time profile (b) are presented. In Fig. 2 the time scale goes with incident shock wave arrival, however, the working conditions are achieved only behind the reflected shock wave so below for all the data presented time scale goes starting from the moment of reflected shock wave arrival. The time interval applicable for the measurements was confined by gas-dynamic perturbation and varied with the incident shock wave velocity. The minimal time accessible for measurements among all the range of investigated conditions was equal to 700 μ s. The error of measurements depended on the signal-to-noise ratio and the difference between the temperature of reactive mixture and the brightness temperature of reference source T_0 . The value of T_0 was varied in the range of 1970–2260 K. The total error of temperature measurements was amounted to 5%.

The used method of the temperature measurements is valid as long as conditions are invariant throughout the observed volume and until the particle absorption is predominated over the scattering. The former condition is fulfilled in the shock tube when the boundary effects or the deposition of particles on the windows with their further cooling-down process can be neglected. According to

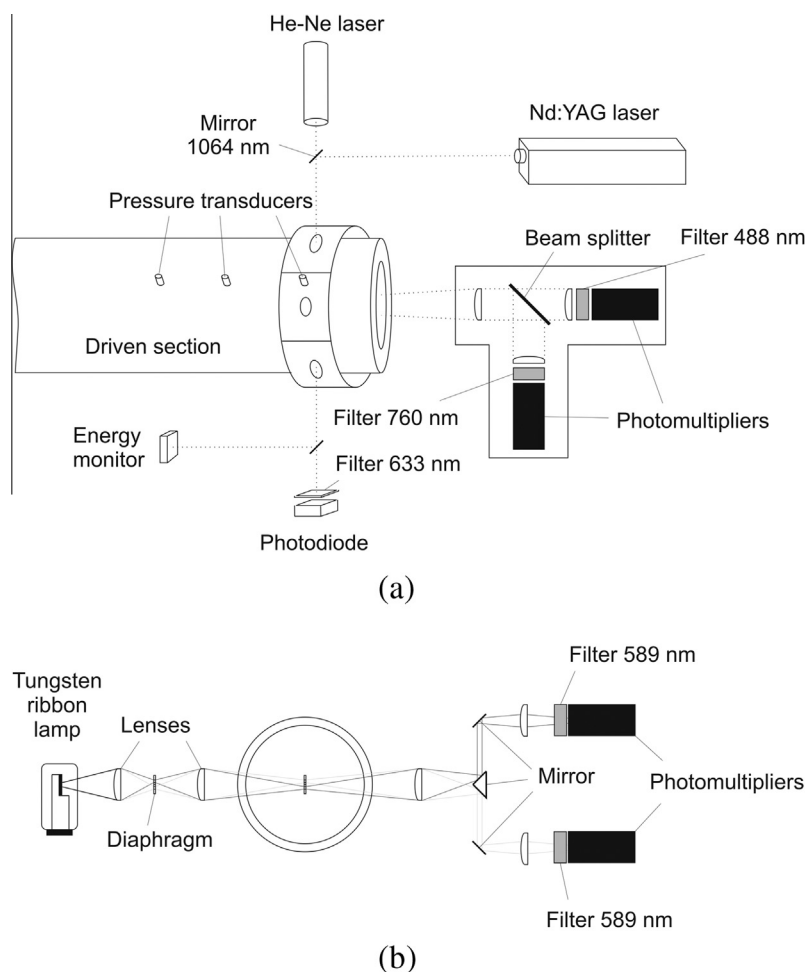


Fig. 1. Experimental setup: the shock tube and optical diagnostics.

Table 1
Experimental conditions.

Mixture label	Mixture composition	Range of T_5 , K	Range of P_5 , bar
1BEN	1% C_6H_6 + 99% Ar	1643–2558	1.4–4.6
2BEN	2% C_6H_6 + 98% Ar	1642–2577	1.5–3.6
3EtOH	3% C_2H_5OH + 97% Ar	1740–2206	3.4–4.8
1BEN1EtOH	1% C_6H_6 + 1% C_2H_5OH + 98% Ar	1732–2616	3.5–5.5
1BEN3EtOH	1% C_6H_6 + 3% C_2H_5OH + 96% Ar	1803–2265	3.3–4.7

special analysis performed for similar experimental parameters in [6], these effects become noticeable approximately at the latest reaction times, comparable with gasdynamic limitations ($\sim 700 \mu s$), i.e. were excluded from consideration. The latter condition can be safely assumed as long as the size of carbon particles is much less than diagnostic wavelength, i.e. within the Rayleigh limit.

2.3. Ti-Re LII particle sizing

The time-resolved laser-induced incandescence (Ti-Re LII) technique was applied for particle sizing. The Ti-Re LII is widely used for particle size measurements in flames [14–16] and shock tubes [2]. The Ti-Re LII technique is based on the particle heating with a laser pulse and the measurement of resulting thermal radiation of the particles. The particle sizes are determined by the analysis of the decay time of laser induced incandescence signals as the larger particles need longer time to cool down than the smaller ones.

The Nd:YAG laser LQ-129 (SOLAR Laser Systems), which operates at a wavelength of 1064 nm with pulse duration of 12 ns FWHM, was applied for the particle heating. The registration of Ti-Re LII signals was performed through a quartz end plate of the shock tube situated at a distance of 45 mm from the laser beam line passing through the vertically installed pair of calcium fluoride windows (Fig. 1a). The LII signals were detected using two narrow band pass filters, centered at the wavelengths of 488 and 760 nm with a Hamamatsu H6780-20 photomultiplier module (rise time 0.78 ns) coupled to a LeCroy WaveRunner 6060A oscilloscope (500 MHz bandwidth). The Nd:YAG laser was triggered by a pressure transducer through a time delay generator. The laser fluence was varied in the range of 0.45–0.5 J/cm².

The particle size was determined by approximation of the experimental Ti-Re LII trace obtained at the wavelength 488 nm with the theoretical curve derived from LII model [17] (see Fig. 3). The measured Ti-Re LII signal was fitted by calculated curves obtained by variation of the count median diameter and at constant value of the standard deviation $\sigma = 1.1$ in the lognormal distribution function using the least-squares method. The LII model, the method of evaluation of mean particle size and estimation of measurement error are described in detail in [17]. The following main assumptions are assumed. Due to absence of reliable data concerning carbon particle properties the data of graphite for heat capacity and density have been used. The optical properties were assumed to be invariable for particle in process of their formation. The particles were considered as the spheres and possible agglomeration process was not been taken into account. The

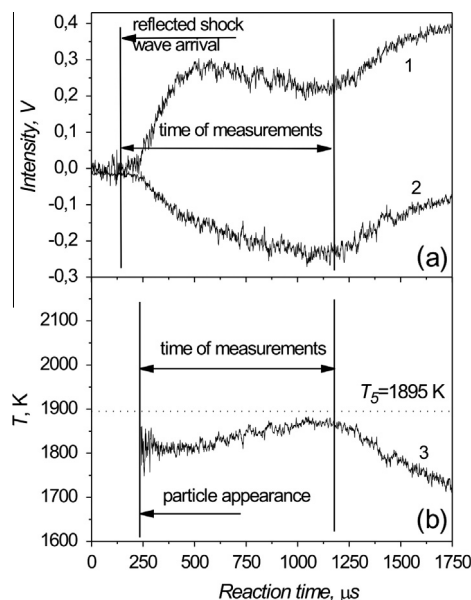


Fig. 2. The signals of emission + absorption (curve 1) and emission (curve 2) (a) and the corresponding temperature profile (curve 3) (b), measured in pyrolysis of mixture 1BEN (see Table 1) at the initial temperature behind the reflected shock wave $T_5 = 1895$ K (dotted line) and at the pressure $p_5 = 3.9$ bar.

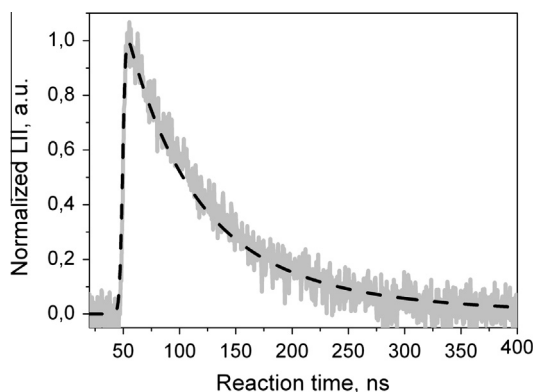


Fig. 3. Normalized experimental LII signal (noise curve) measured at wavelength of 488 nm in pyrolysis of mixture 1BEN at $T_5 = 2078$ K and $p_5 = 3.5$ bar and calculated curve (dash line) obtained with LII model [17].

uniform heating of particles by laser irradiation was assumed. The uncertainties of the particle properties (density, heat capacity, accommodation coefficient) and of the experimental conditions (gas temperature, pressure, laser fluence) lead to the systematic errors of the measured values of particle diameter. A detailed error calculation for all values results in an estimated overall uncertainty from -26% up to $+23\%$.

2.4. Extinction measurements

A measurement of extinction time profile is one of the most informative methods of investigation of the processes of overall volume fraction of condensed phase formation behind shock waves and in flames, which was used in a number of works [1–8,14]. The beam of a conventional 20 mW HeNe laser was passed through two calcium fluoride windows of the shock tube (Fig. 1a) and focused on the active photo-detector PDA10A-ES (THORLABS) with a rise time of 10 ns. The detector was optically blocked by an interference filter of $\lambda = 632.8$ nm (FWHM 1 nm) to suppress the thermal radiation of the reacting gas-particle mixture. The signal

from the detector was recorded on Tektronix TDS 2014B digital scope with 100 MHz pass band width. In Fig. 4a an example of extinction signal is presented. Particle extinction, determined by the attenuation of passing radiation, is linked with the volume fraction of condensed phase by Lambert-Beer's law:

$$f_v(t) = \frac{\ln\left(\frac{I(t)}{I_0}\right)\lambda}{-6\pi E(m) \cdot l} \quad (2)$$

here t – is the reaction time, I_0 and I – are the incoming and transmitted laser light intensities respectively, λ – is a diagnostic wavelength, l – is the optical path length, $E(m)$ – is the refractive index function of particle material, which is a priori unknown and in general is dependent on the diagnostic wavelength [14,15] and the carbon particle size [16,17]. Therefore in the present analysis the product of volume fraction of condensed phase f_v and the function of refractive index $E(m)$:

$$f_v(t) \cdot E(m) = \frac{\ln\left(\frac{I(t)}{I_0}\right)\lambda}{-6\pi \cdot l} \quad (3)$$

was analyzed, below it is called as “relative volume fraction”. The example of time profile of evaluated relative volume fraction of condensed phase is shown in Fig. 4b.

The extinction measurements also allow analyzing the main kinetic characteristics of condensed phase: the induction time of particle inception and the rate constant of particle growth. The absolute value of the induction time t_{ind} was defined as the intersection of the inflectional tangent of the carbon particle volume fraction profile with the time axis (see Fig. 4b). The stage of the process following the induction time is characterized by the rapid growth of volume fraction of condensed phase. This process according to [3,18] could be well described by the equations of relaxation type:

$$\frac{df_v}{dt} = k_f \cdot (f_v^\infty - f_v(t)) \quad (4)$$

Here f_v^∞ – is the final observed value of volume fraction of condensed phase, k_f – is an effective rate constant of particle growth. This approach was applied to the treatment of the time profiles of relative volume fraction of condensed phase, an example of such treatment one can see in Fig. 4b.

3. Experimental results

In Fig. 5 the examples of simultaneously measured temperature (curve 1), relative volume fraction of condensed phase $f_v \times E(m)$ (curve 4) and particle size (dots 5 – experimental data, curve 6 – best fit of 5) time profiles for initial temperature ranges $T_5 = 1728$ – 1770 K, $T_5 = 1913$ – 1988 K, $T_5 = 2086$ – 2148 K in pyrolysis of mixture 1BEN (see Table 1) are presented. The temperature and extinction time profiles were measured in each experiment while LII sizing was performed in one particular moment in one experiment. Thus for presentation of the particle size time profiles the experiments with different LII delays from the reflected shock wave were collected in one plot while the temperature T_5 was slightly varied from shot to shot. The sharp peaks at temperature and extinction signals reflect the moment of Nd:YAG laser pulse. Zero time corresponds to the moment of reflected shock wave arrival in the measurement cross section. The temperature measurements (curve 1) started only with the moment of appearance of considerable amount of condensed phase. Initial temperatures T_5 behind the reflected shock wave are presented by the dash lines (curve 2). The maximal possible temperature drop caused by the heat consumption of decomposition of initial hydrocarbons in investigated conditions was evaluated by the kinetic modeling

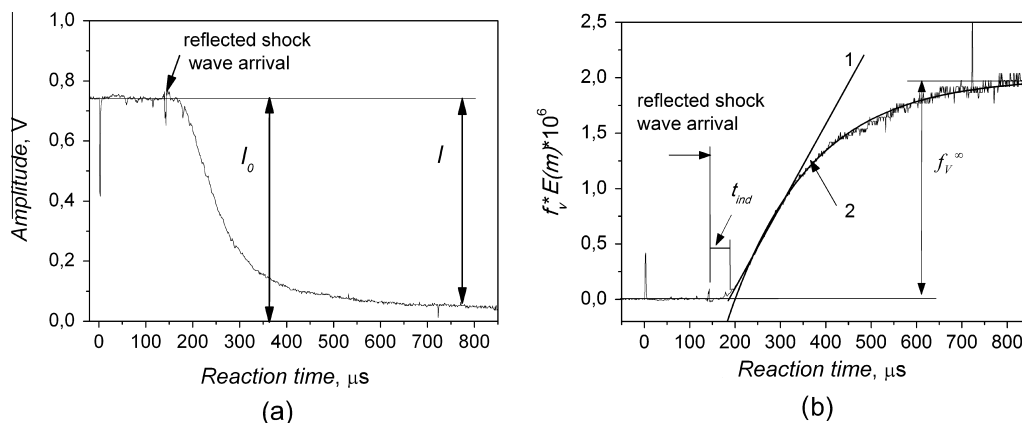


Fig. 4. The extinction signal measured at wavelength 633 nm in mixture 1BEN at $T_5 = 2064$ K and $p_5 = 3.8$ bar (a) and the corresponding relative volume fraction of condensed phase time profile evaluated by Eq. (3) (b). Line 1 – is the inflectional tangent of $f_v \times E(m)$ time profile, curve 2 – is the approximation curve for the $f_v \times E(m)$ time profile.

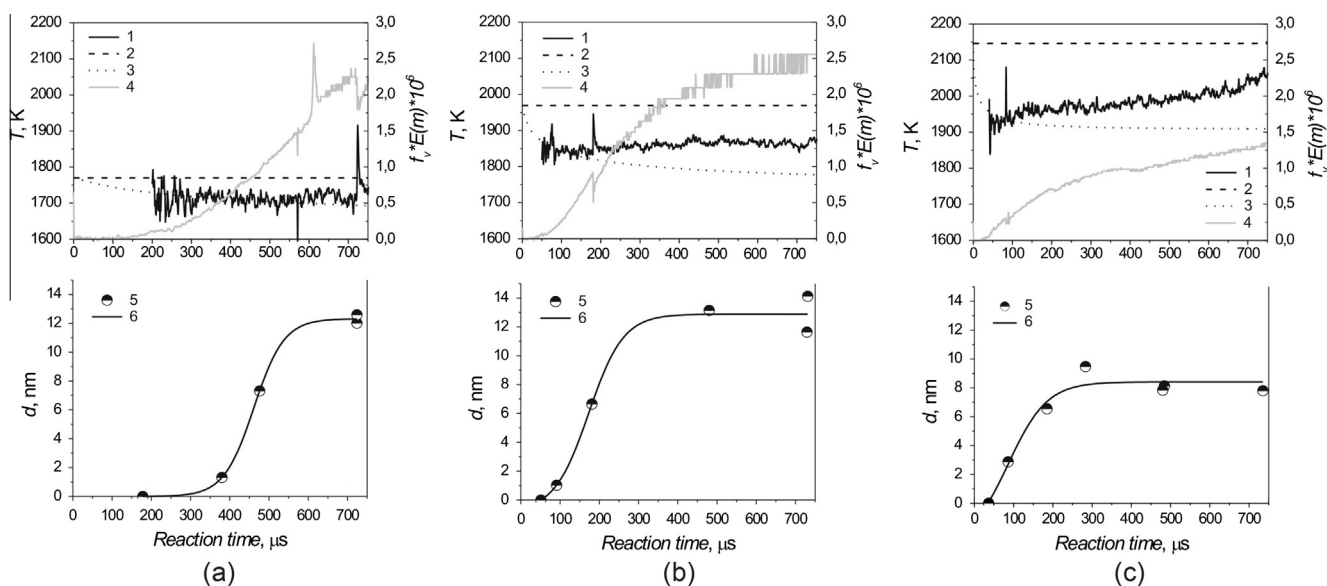


Fig. 5. Temperature, relative volume fraction of condensed phase (above) and particle size (below) time profiles measured in pyrolysis of mixture 1BEN: 1 – measured temperature; 2 – initial frozen temperature behind the reflected shock wave – T_5 ; 3 – calculated temperature accounting only the endothermics of hydrocarbons decomposition – T_{calc} ; 4 – relative volume fraction of condensed phase – $f_v \times E(m)$; 5 – carbon particle size – d ; 6 – best fit of 5. Initial temperatures behind the reflected shock wave at the size measurements (lower plots): (a) $T_5 = 1728$ – 1770 K, (b) $T_5 = 1913$ – 1988 K and (c) $T_5 = 2086$ – 2148 K.

and presented by the dot lines (curve 3). The calculations were carried out using the CHEMKIN code and the kinetic mechanism consisting of 40 major reactions of benzene and phenol decomposition taken from [19] and additional 56 reactions for ethanol decomposition and 20 reactions of hydrogen–oxygen sub-mechanism taken from [20]. The tables with the kinetic mechanisms are included in [supplement material #2](#). Note that the reactions of PAH and soot growth proceeding during the observed reaction time were not considered in kinetic modeling. Thus the calculated temperature T_{calc} , taking into account only endothermic effect of thermal decomposition of initial hydrocarbons, represented the lower estimation of real temperature.

In pyrolysis of more rich mixture 2BEN the extinction signal was oversaturated in the range of maximum of relative volume fraction $f_v \times E(m)$ (the center of bell-shaped dependence, see below, Fig. 7) and incandescence of laser-heated particles was absorbed by the unheated particles between the investigation section and the end flange (see Fig. 1a). Therefore for this mixture no unambiguous data about particle size was extracted. Nevertheless temperature measurements in this mixture are reliable in all

regimes. In pyrolysis of the mixture 3EtOH no soot formation was observed in all temperature regimes. Time profiles of temperature and extinction measurements for different pyrolysis regimes for 2BEN, 1BEN1EtOH and 1BEN3EtOH mixtures are presented in [supplement material #3](#).

4. Analysis of experimental data

4.1. Temperature trend in benzene and benzene–ethanol pyrolysis

The difference between the measured temperature T_{meas} and the initial temperature T_5 at the reaction time of $700 \mu s$ in dependence on T_5 for various mixtures is presented in Fig. 6a. The deviation of the measured temperature from the initial one ($T_{meas} - T_5$) increased towards higher values of T_5 owing to the increase of a degree of benzene decomposition. The maximal temperature drop, corresponding to significant decomposition of benzene (80% at $T_5 = 1900$ K, see calculation of benzene decomposition in dependence on temperature in [supplementary material #3](#)) was equal to 120 K and 300 K for the mixtures 1BEN and 2BEN respectively.

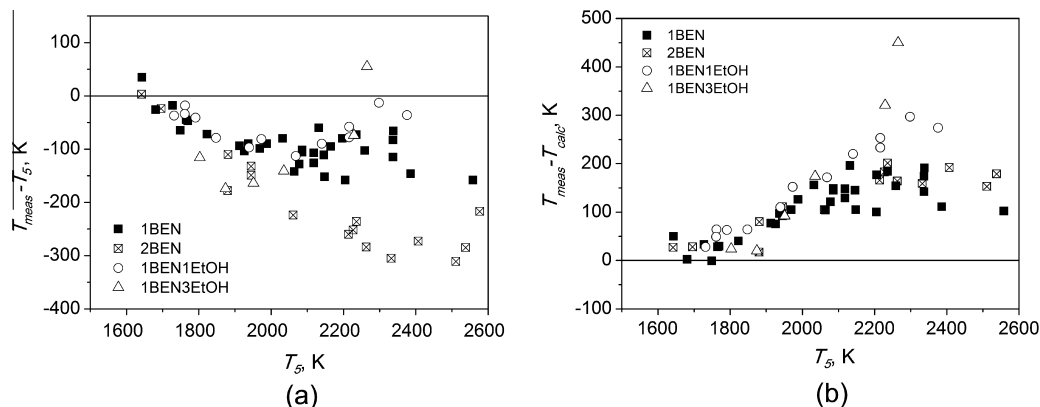


Fig. 6. The difference between the measured T_{meas} and the initial T_5 temperatures (a), and between T_{meas} and calculated temperature T_{calc} (b) at the reaction time of 700 μs for various mixtures in dependence on the initial temperature behind the reflected shock wave T_5 .

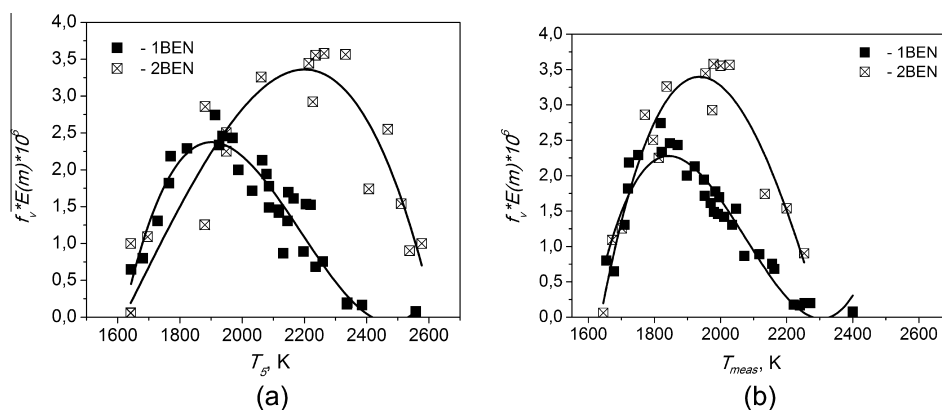


Fig. 7. Bell-shaped temperature dependence of relative volume fraction of condensed phase in the pyrolysis of 1BEN and 2BEN mixtures: (a) data presented versus the initial temperature behind the reflected shock wave T_5 , and (b) data presented versus the measured temperature at the reaction time of 700 μs , continuous curves – fit of the experimental data with cubic polynomial.

With the further increase of initial temperature the value of $(T_{\text{meas}} - T_5)$ remained constant for the mixtures of benzene without ethanol addition. In the pyrolysis of mixture 3EtOH no condensed phase was observed and therefore temperature measurements were not carried out. In the benzene–ethanol mixtures (1BEN1EtOH and 1BEN3EtOH) the difference $(T_{\text{meas}} - T_5)$ at low initial temperatures ($T_5 < 1900$ K) showed the same behavior as in the mixtures 1BEN and 2BEN. For higher temperatures ($T_5 > 1900$ K) the measured temperatures T_{meas} showed a gradual increase (1BEN1EtOH and 1BEN3EtOH mixtures).

From Fig. 5b and c one can see that the measured temperature T_{meas} is significantly higher than the calculated temperature T_{calc} . The excess of the measured temperature over the calculated one $(T_{\text{meas}} - T_{\text{calc}})$ at the reaction time of 700 μs is presented in Fig. 6b in dependence on T_5 . It was found that the temperature rise reached a constant value starting from the temperature $T_5 = 1900$ K (corresponding to 80% decomposition of benzene) for the mixtures without ethanol addition (see Fig. 6b). In the mixtures with ethanol the value of $(T_{\text{meas}} - T_{\text{calc}})$ continuously raised with the increase of T_5 .

4.2. Temperature dependence of relative volume fraction of condensed phase

In Fig. 7 the temperature dependence of relative volume fraction of condensed phase measured at the reaction time of 700 μs in pyrolysis of 1BEN and 2BEN mixtures is presented. In Fig. 7a the data $f_v \times E(m)$ (Eq. (3)) are presented in dependence on initial temperature behind the reflected shock wave T_5 . It is seen that

the shift of maximal value of relative volume fraction from 1900 K for 1BEN to 2210 K for 2BEN is notable. Similar shift to higher temperatures of the top of bell-shaped curves plotted versus the frozen temperature T_5 with the increase of initial hydrocarbon concentration was found in other studies [2–4]. The plot on Fig. 7b represents the dependence of relative volume fraction on the real gas–particle temperature measured at the same reaction time of 700 μs . In this case the shift of maximal value of $f_v \times E(m)$ is insignificant. Thus the shift of bell-shaped temperature dependence of relative volume fraction of condensed phase is determined by the temperature change due to heat consumption of hydrocarbons decomposition and heat release of condensation.

4.3. Ethanol admixture influence on soot formation

In Fig. 8a the relative volume fraction of condensed phase measured at the reaction time of 700 μs in pyrolysis of the mixtures 1BEN, 1BEN1EtOH and 1BEN3EtOH is presented in dependence on the current temperature. The position of the top of bell-shaped curve did not change with ethanol addition. The maximum value of relative volume fraction of condensed phase shows the slight growth for mixture 1BEN1EtOH relatively to the value for 1BEN. This result is in agreement with observations [4] where the increase of soot amount in shock tube pyrolysis of 1% $\text{C}_7\text{H}_8 + (1-3)\% \text{C}_2\text{H}_5\text{OH} + \text{He}$ was found. But with the following increase of ethanol addition (mixture 1BEN3EtOH) the value of relative volume fraction of condensed phase again decreased and became the same as in the mixture without ethanol – 1BEN.

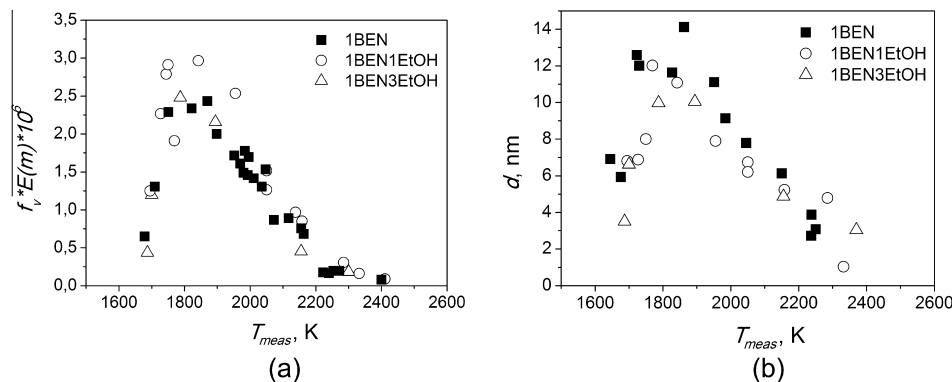


Fig. 8. The bell-shaped temperature dependences of relative volume fraction of condensed phase (a) and size of soot particles (b) formed during pyrolysis of various mixtures.

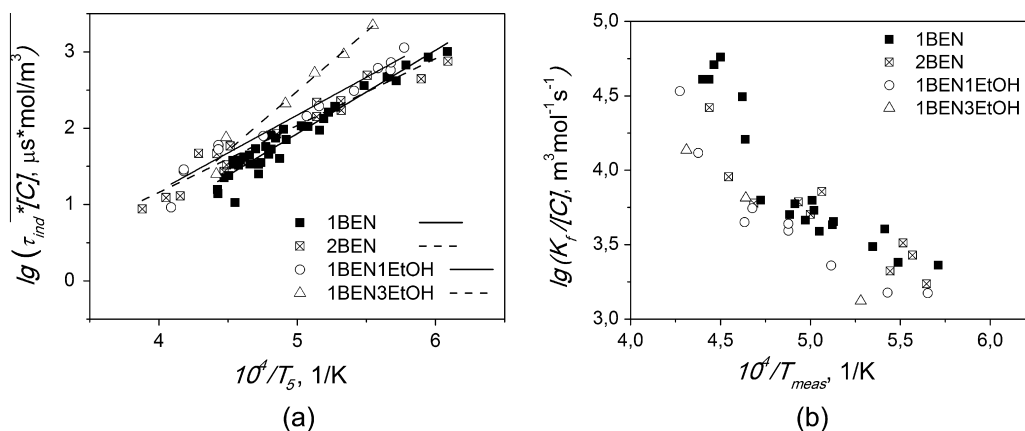


Fig. 9. Induction times of carbon particle inception (a) and the rate constants of condensed phase growth (b) observed in pyrolysis of various mixtures.

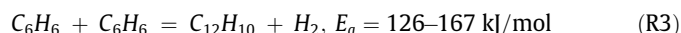
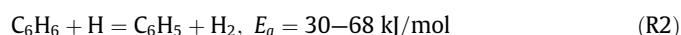
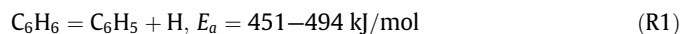
The similar bell-shaped temperature dependence of the particle size measured by the LII at the same reaction time was found and presented in Fig. 8b. The slight suppression effect of ethanol admixture on the particle size was observed especially in case of mixture 1BEN3EtOH. However one should take into account that the significant error for particle sizing by LII reaches to +23%/–26%. Thus, the suppression effect of ethanol addition based on LII measurements is quite questionable.

4.4. Kinetic characteristics of the particle formation process: the induction time of particle inception and the rate constant of particle growth

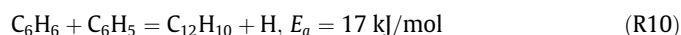
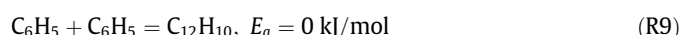
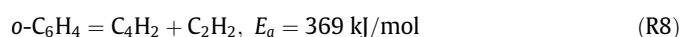
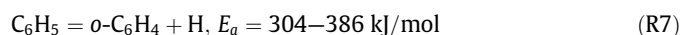
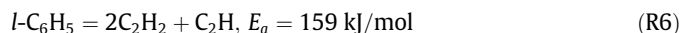
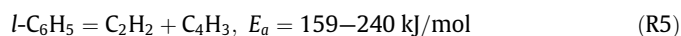
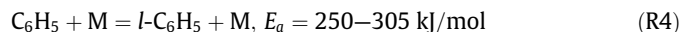
In Fig. 9a the induction times of particle inception t_{ind} in the pyrolysis of benzene mixtures with addition of ethanol are presented in dependence on the initial temperature T_5 . The data were normalized to total carbon atom concentration in the first power as recommended in [3]. Besides experimental dots the lines of fitting are presented. The initial temperature behind the reflected shock wave was used since the initial reactions start at this temperature. The induction time of appearance of condensed particles is determined by the rates of early stages of the pyrolysis, namely the endothermic reactions of primary molecules decomposition and initial polymerization of products of dissociation. Therefore the temperature dependence of t_{ind} , as a rule, well obeys to Arrhenius law, i.e. exponentially decreases with temperature rise [3]. The slope of the temperature dependence of the induction time in Arrhenius coordinates reflects the effective activation energy of these initial endothermic reactions. One can expect that the reaction with the higher activation energy would make a main contribution in the slope of temperature dependence of induction time.

The activation energy extracted from the linear slope of temperature dependence of induction time was found to be 210 kJ/mol for 1BEN, 168 kJ/mol for 2BEN, 193 kJ/mol for 1BEN1EtOH and 300 kJ/mol for 1BEN3EtOH.

The reactions of benzene decomposition were considered following to [21]:



The decomposition of phenyl proceeds through the reactions:



The values of extracted effective activation energies for mixtures of benzene (1BEN, 2BEN) are considerably lower than those for initial reactions of benzene and phenyl decomposition ((R1) and (R4)). That is probably the evidence that the main kinetic

pathway proceeds through the reaction (R3). The reason of observed decrease of effective activation energy with increase of initial benzene concentration (mixture 2BEN in comparison with 1BEN) is also the partial influence of the reaction (R3). The admixture of 1% C_2H_5OH to 1% C_6H_6 (1BEN1EtOH) diluted in Ar did not change significantly the slope of induction time plot. With the admixture of 3% C_2H_5OH the noticeable increase of the absolute values and the activation energy of induction time of particle inception were observed (see Fig. 9a).

The stage of process following the induction time is characterized by the fast growth of extinction and, thus, reflects a sharp increase in volume fraction of condensed phase. Extinction measurements do not allow determining, with what effect the increase of f_v is connected with increase in number of particles, their sizes or with change of their refractive index. Nevertheless, the evidence of f_v rise presents the important phenomenological characteristic of process of particle formation, which is quite valuable for the elaborating of kinetic mechanisms of particle surface growth. In Fig. 9b the Arrhenius dependence of the rate constants of particle growth k_f (4) on the measured temperature T_{meas} are presented. The experimentally determined values of this rate constant were plotted versus the current values of measured temperature as the temperature changed essentially during the time of particle growth (see Fig. 5). In Fig. 9b one can see that the rate constant k_f steeply increases with the temperature, while the admixture of ethanol causes the noticeable decrease of k_f .

5. Discussion

Firstly, it should be noted the essential deviation of the temperature from the initial value behind the reflected shock wave even in the mixtures containing only 1% of benzene in argon (see Figs. 2, 5 and 6). This fact results in the change of kinetics of condensed particle growth and extracted temperature dependences of relative volume fraction of condensed phase and particle size. The measured temperature profiles demonstrate the different behavior during the reaction time in the pyrolysis of benzene at the different initial temperatures T_5 (see Fig. 5). At low temperature conditions $T_5 = 1728\text{--}1770\text{ K}$ (Fig. 5a) the decomposition of benzene progressed slowly and, as it was found by calculations, the degree of decomposition at the reaction time of 250–300 μs did not exceed 30%. Thus, the long induction time of particle inception was observed and the time-behavior of the temperature of the mixture was conditioned by the endothermic effect of benzene decomposition. At $T_5 = 1913\text{--}1988\text{ K}$ (Fig. 5b) the temperature is nearly constant during the reaction time that one could consider as the evidence of balancing of the heat effects of benzene decomposition and carbon condensation. At $T_5 = 2086\text{--}2148\text{ K}$ (Fig. 5c) the benzene decomposes completely at first 50–100 μs that leads to considerable temperature drop during this time. The following gradual temperature increase one can regard to the heat release of carbon particle formation.

As it is expected, the greater benzene concentration the greater the difference of ($T_{meas} - T_{calc}$) (see Fig. 6b) as the larger amount of carbon atoms is involved in condensation process. The addition of 3% ethanol to the 1% benzene in argon (mixture 1BEN3EtOH) leads to significant increase of this difference. Note, that the calculated temperature drop owing to thermal decomposition of hydrocarbons was approximately the same for the mixtures 2BEN and 1BEN3EtOH. Thus, the additional temperature increase in the pyrolysis of mixtures with ethanol, well seen in Fig. 5a, could be regarded to the exothermic reactions with the products of ethanol decomposition. In fact, the calculations of species concentration during the initial stages of pyrolysis of the mixtures 1BEN1EtOH and 1BEN3EtOH are resulted in formation of H_2O , which is absent

in the benzene pyrolysis. Thus, the exothermics of reaction of H_2O formation could be the probable reason of additional temperature rise in the pyrolysis of the mixtures with ethanol addition.

It is remarkable that the positions of the top of bell-shaped curves of temperature dependences of particle volume fraction and size practically do not change with the change of benzene concentration and addition of ethanol when the real temperature T_{meas} is used for the analysis instead of the “frozen” temperature T_5 (see Figs. 7 and 8).

Analyzing the obtained dependences one can conclude that the rise of the final values of relative volume fraction of condensed phase and particle size with the temperature increase on the left-hand branch of the bell-shaped curves (see Figs. 7 and 8) corresponds to an increase of degree of benzene decomposition. The top of bell-shaped dependences of the relative volume fraction of condensed phase and particle size is located at the temperatures about 1900 K. At these temperatures, according to the calculations carried out using the kinetic mechanism [19], 80% of initial benzene decomposes. With the further temperature rise corresponding to the right-hand branch of the bell-shaped curves the degree of precursor decomposition does not change, but the rate of its decomposition increases. Presumably the rise of concentration of active radicals results in the fast formation of large amount of particle nuclei and consequently leads to the smaller final size of carbon particles. In view of this, the apparent decrease of the particle volume fraction (measured at 633 nm) at high temperatures could be explained by a fall of particle absorption at this wavelength with the decrease of their size [15,16].

6. Conclusions

A multi-channel optical diagnostic for real temperature measurements, particle extinction measurements and particle sizing was applied for observation of carbon particle formation process in a pyrolysis of benzene and benzene–ethanol mixtures behind reflected shock waves.

The drastic drop of the measured temperature due to decomposition of initial hydrocarbon molecules increasing towards higher initial temperatures and the following temperature rise due to particle condensation process were observed in benzene pyrolysis. The position of maximum of bell-shaped temperature dependence of final value of volume fraction of condensed phase should be determined by the value of real temperature, eventuated from heat consumption of hydrocarbons decomposition and heat release of condensation. It was shown that for correct analysis of the temperature dependences of carbon particle growth in hydrocarbon pyrolysis the current measured temperature has to be used.

At initial temperatures $T_5 < 1900\text{ K}$ the behavior of the measured temperature during pyrolysis was similar for both pure benzene and benzene–ethanol mixtures. Whereas for $T_5 = 1900\text{--}2400\text{ K}$ the significant additional heat release in pyrolysis of benzene–ethanol mixtures was found. The probable reason of this phenomenon is the exothermic reactions of H_2O formation occurring in the reactive mixture.

In pyrolysis of the mixture 3% C_2H_5OH no soot formation was observed in all temperature regimes. The increase of relative volume fraction of carbon particles with small admixture of ethanol in benzene was observed while with the increase of ethanol percentage the same value of final value of volume fraction of condensed phase as in pure benzene mixtures was observed. The slight suppression effect of ethanol admixture on the particle size was also detected. The slope of induction time plot is not noticeably changed by admixture of 1% C_2H_5OH to 1% C_6H_6 diluted in Ar. With the admixture of 3% C_2H_5OH the noticeable increase of the absolute values and the activation energy of induction time of particle

inception were observed. The values of extracted effective activation energies for mixtures of benzene are considerably lower than those for reactions of benzene and phenyl decomposition. That is the evidence of main kinetic pathway proceeds through the reaction of direct benzene molecules recombination.

Presented results could be useful for the elaborating of kinetic mechanisms of particle surface growth.

Acknowledgment

This work was supported by the RFBR projects 13-08-00454 and 14-08-00505.

Appendix A. Supplementary material

Supplementary data associated with this article can be found, in the online version, at <http://dx.doi.org/10.1016/j.combustflame.2014.09.015>.

References

- [1] M. Frenklach, D. Clary, W. Gardiner, S. Stein, *Proc. Combust. Inst.* 20 (1984) 887–901.
- [2] R. Starke, P. Roth, *Combust. Flame* 127 (2002) 2278–2285.
- [3] A. Eremin, *Prog. Energy Combust. Sci.* 38 (2012) 1–40.
- [4] A. Alexiou, A. Williams, *Combust. Flame* 104 (1996) 51–65.
- [5] I. Zhil'tsova, I. Zaslonko, Y. Karasevich, et al., *Kinet. Catal.* 41 (2000) 76–89.
- [6] A. Emelianov, A. Eremin, A. Makeich, H. Jander, H. Gg Wagner, R. Starke, C. Schulz, *Proc. Combust. Inst.* 31 (2007) 649–656.
- [7] K. Ishii, N. Ohashi, A. Teraji, M. Kubo, in: *Proc. of 22nd ICDERS*, 2009.
- [8] M. Frenklach, T. Yua, in: *Proc. XVI Int. Symp. on Shock Tubes and Waves*, 1987, pp. 487–493.
- [9] J. Wu, K. Song, T. Litzinger, S.-Y. Lee, R. Santoro, M. Linevsky, M. Colket, D. Liscinsky, *Combust. Flame* 144 (2006) 675–687.
- [10] H. Böhm, M. Braun-Unkloff, *Combust. Flame* 153 (2008) 84–96.
- [11] C. McEnally, L. Pfefferle, *Proc. Combust. Inst.* 31 (2007) 603–610.
- [12] A. Gaydon, I. Hurler, *Shock Tube in the Chemical Physics of High Temperatures*, Chapman and Hall Ltd., London, 1963.
- [13] L.A. Melton, *Appl. Opt.* 23 (1984) 2201–2208.
- [14] S. De Iuliis, F. Migliorini, F. Cignoli, G. Zizak, *Appl. Phys. B: Lasers Opt.* 83 (2006) 397–402.
- [15] C. Schulz, B.F. Kock, M. Hofmann, H. Michelsen, S. Will, B. Bougie, R. Suntz, G. Smallwood, *Appl. Phys. B: Lasers Opt.* 83 (2006) 333–354.
- [16] H. Bladh, J. Johnsson, N.-E. Olofsson, A. Bohlin, P.-E. Bengtsson, *Proc. Combust. Inst.* 33 (2011) 641–648.
- [17] A. Eremin, E. Gurentsov, E. Popova, K. Priemchenko, *Appl. Phys. B: Lasers Opt.* 104 (2011) 285–295.
- [18] B. Haynes, H. Wagner, *Zeit. Phys. Chem.* 133 (1982) 201–213.
- [19] C. Saggese, A. Frassoldati, A. Cuoci, T. Faravelli, E. Ranzi, *Combust. Flame* 160 (2013) 1168–1190.
- [20] N. Marinov, *Int. J. Chem. Kin.* 31 (1999) 183–220.
- [21] kinetics.nist.gov.